water

MDPI

Supplementary Materials

Enhanced Ozone Oxidation by a Novel Fe/Mn@γ−Al2O3 Nanocatalyst: The Role of Hydroxyl Radical and Singlet Oxygen

Chen Liang [1,2], Xinhao Luo [1,2] and Yongyou Hu [1,2,*]

Text S1. Steady−state Concentrations of Different Reactive Species

O_3. Ozone concentration was determined by the indigo method as described in previous studies [1,2].

HO°. Nitrobenzene (NB) as the HO° probe compound was selected for determining the steady−state concentration of HO° ($[HO^\circ]_{SS}$). NB reacts selectively with HO° (k_{NB, HO°= 3.9×10^9 M^{-1} s^{-1}), much higher than those of O_3 (k_{NB, O_3}=9×10^{-2} M^{-1} s^{-1})[3] and $^1O_2$ ($k_{NB, {}^1O_2}$ = 5×10^3 M^{-1} s^{-1}) [4]. NB (5.0 μM) was added to the O_3−catalyst system and the concentration of NB was determined at specified time intervals. $[HO^\circ]_{SS}$ was then estimated based on Equations S1−S2:

$$-\ln\left(\frac{[NB]_t}{[NB]_0}\right) = k_{NB, HO^\circ}[HO^\circ]_{SS} \times t \quad \text{(S1)}$$

$$k'_{NB} = k_{NB, HO^\circ} \times [HO^\circ]_{SS} \quad \text{(S2)}$$

where [NB] is the concentration of NB, k_{NB, HO° is the second−order rate constant between HO° and NB, and k'_{NB} represents the observed first−order rate constant of NB in the O_3−catalyst process. NB was determined by using a UPLC system with a PDA detector at a wavelength of 265 nm.

$^1O_2$. Furfuryl alcohol (FFA) was selected as the probe of singlet oxygen ($^1O_2$) to estimate its steady−state concentration ($[^1O_2]$). Both $^1O_2$ ($k_{FFA, {}^1O_2}$ = 1.3×10^8 M^{-1} s^{-1})[5,6] and HO° (k_{FFA, HO°= 1.5×10^{10} M^{-1} s^{-1}) [7] can react with FFA with a high rate constant, but FFA resists with O_3 [3,5]. Thus, $[^1O_2]_{SS}$ was estimated based on Equations S3−S4 with the aforementioned $[HO^\circ]_{SS}$:

$$-\ln\left(\frac{[FFA]_t}{[FFA]_0}\right) = (k_{FFA, HO^\circ}[HO^\circ]_{SS} + k_{FFA, {}^1O_2}[{}^1O_2]_{SS}) \times t \quad \text{(S3)}$$

$$k'_{FFA} = k_{FFA, HO^\circ} \times [HO^\circ]_{SS} + k_{FFA, {}^1O_2} \times [^1O_2]_{SS} \quad \text{(S4)}$$

where [FFA] is the concentration of FFA, $k_{FFA, HO^\circ}$is the second−order rate constant between $^1O_2$ and NB, and k'_{FFA} represents the observed first−order rate constant of FFA in the O_3−catalyst process. FFA was determined by using a UPLC system with a PDA detector at a wavelength of 214 nm.

Text S2. Determination of the Rate Constant of DMP with HO°

The second−order rate constants for the reaction of DMP with HO° was determined by using 266 nm laser flash photolysis. The spectra of DMP aqueous solutions were examined after filtration and no significant signal was observed. Different concentrations of DMP were added into 100 mM H_2O_2 served as HO° precursor (Equation S5).

$$H_2O_2 + h\nu \rightarrow 2HO^{\circ} \quad (5)$$

HO°−adducts were generated from HO° addition to the aromatic ring of DMP (Equation S6) [8], and the maximum absorption of was observed at 320 nm.

$$DMP + HO^{\circ} \rightarrow DMP{-}OH \quad (6)$$

Thus, the second−order rate constants were determined by monitoring the build−up traces of $HO^{\bullet}$−adducts at 320 nm (Figure S10). The first−order build−up rate constants against DMP concentrations (0.05−0.3 mM) are linear and the slope is the value of the second−order rate constant (i.e., $3.7 \pm 0.3 \times 10^9$ M^{-1} s^{-1}). This is consistent with the rate constant reported previously [8,9].

Text S3. Factors Influencing Catalytic Performance

Experimental Procedure

The catalyst optimization and the effects of the water matrix on the pollutant removal were investigated. The experiment procedure was conducted as described in Section 2.3. The molar ratio of Fe/Mn on the catalyst and the catalyst dosage were selected to optimize the catalytic activity. Specifically, the molar ratios of Fe/Mn with catalyst dosage of 200 mg L^{-1} were set at 0.3, 0.6, 1, 1.5, and 3. The catalyst dosages with molar ratios of 1.5 were set at 50, 100, 150, 200, 300, respectively. The anions including sulfate, chloride, carbonate, and nitrate with 2 mM, pH value (5–9), and real water samples including printing and dyeing industrial park secondary effluent (PDIP) effluent, wastewater treatment plant (WWTP) effluent, and river water (RW) were selected to evaluate the effect of the water matrix on the performance of the Fe/Mn@γ−Al_2O_3/O_3 system. The molar ratios of Fe/Mn and catalyst dosage were set at 1.5 and 200 mg L^{-1}.

Effect of the Molar Ratio of Fe/Mn

As seen in Figures S5B and S5D, catalysts with various Fe/Mn ratios exhibited different catalytic activities. The removal of 1−NP and DMP from the surface of the catalyst was not affected by the ratio of Fe/Mn and was less than 10%. It showed that Fe/Mn@γ−Al_2O_3 with the ratio of Fe to Mn at 3:2 displayed the best catalytic activity. The leaching concentrations of Fe, Mn, and Al ions in the system after reaction were determined by ICP−OES. The leaching concentrations of Fe Mn, and Al ions in the solution were very low, even below the detection limit (0.1 mg L^{-1}) in the Fe/Mn@γ−Al_2O_3 catalytic ozonation system. The lower dissolution of the metal components also reflected the structural stability of the catalyst. The reuse test of the catalyst also indicated the stability and durability of this catalyst (Figure S7).

Effect of Catalyst Dosage

The presence of the Fe/Mn@γ−Al_2O_3 catalyst significantly promoted the degradation of 1−NP and DMP during ozonation. The effect of the Fe/Mn@γ−Al_2O_3 dose on the catalytic system was examined in the range of 50 mg/L to 300 mg/L. As seen in Figures S5A and S5C, it was obvious that increasing the dose of Fe/Mn@γ−Al_2O_3 can positively promote the removal of 1−NP and DMP. When the dose of Fe/Mn@γ−Al_2O_3 increased to 300 mg/L, the degradation efficiency of model pollutants showed a trend of inhibition. The catalytic stability of Fe/Mn@γ−Al_2O_3 was also evaluated by batch cycle experiments. Altogether, the results indicated that Fe/Mn@γ−Al_2O_3 has excellent stability and reusability.

Table S1. Dissolution of metal ions in Fe/Mn@γ−Al_2O_3 catalytic ozonation.

	2nd	4th	6th	8th	10th
Fe(mg L^{-1})	0.233	0.328	0.365	0.399	0.413
Mn(mg L^{-1})	0.193	0.203	0.212	0.253	0.264
Al(μg L^{-1})	7.45	7.98	9.12	10.16	12.64

Table S2. The steady−state concentrations of different reactive species.

Compound	Treatment	Steady−state concentrations (M)		
		$[O_3]$	[HO°]	$[^1O_2]$
DMP	O_3	2.4×10^{-5}	2.1×10^{-13}	1.7×10^{-10}
	O_3 + Fe/Mn@Al_2O_3	2.3×10^{-5}	8.1×10^{-13}	1.8×10^{-9}
1−NP	O_3	2.4×10^{-5}	1.1×10^{-13}	2.3×10^{-10}
	O_3 + Fe/Mn@Al_2O_3	2.5×10^{-5}	1.2×10^{-12}	2.0×10^{-9}

Table S3. The reactivity of different probes/quenchers with reactive species.

Compound	The second−order rate constant (M^{-1} s^{-1})			
	O_3	HO°	$^1O_2$	$O_2°^-$
FFA	N.A.[#]	1.5×10^{10} [7]	1.3×10^{8} [5,6]	N.A.[#]
p−BQ	2.5×10^{3} [10]	1.2×10^{9} [11]	N.A.[#]	9.0×10^{8} [12]
NB	9×10^{-2} [3]	3.9×10^{9} [13]	5×10^{3} [4]	N.A.[#]

[#] N.A.: not available.

Table S4. XPS parameters of high−resolution Mn 2p3/2, Fe 2p3/2, and O 1s regions.

	Mn $2p_{3/2}$				Fe $2p_{3/2}$				O 1s					
	Mn(Ⅲ)		Mn(Ⅳ)		Fe(Ⅱ)		Fe(Ⅲ)		O_{MO}		O_{lat}		O_{ads}	
	B.E. (eV)	Ratio[#] (%)	B.E. (eV)	Ratio[#] (%)	B.E. (eV)	Ratio[#] (%)	B.E. (eV)	Ratio[#] (%)	B.E. (eV)	Ratio[#] (%)	B.E. (eV)	Ratio[#] (%)	B.E. (eV)	Ratio[#] (%)
Before reaction	642.2	61.30	643.8	38.70	711.7	37.33	712.9	62.67	531.2	51.36	532.4	27.66	530.3	20.99
After reaction	642.0	50.81	643.4	49.19	711.4	56.54	713.9	43.46	531.4	46.3	532.5	33.31	530.8	20.34

[#]The ratios of Mn(III) or Mn(IV) are calculated by Mn(III/IV)/(Mn(III) + Mn(IV)), Fe(II) or Fe(III) are calculated by Fe(II/III)/(Fe(II) + Fe(III)), O_{MO}, O_{lat} or O_{ads} are calculated by (O_{MO}/O_{lat}/O_{ads})/(O_{MO} + O_{lat} + O_{ads}).

Table S5. Parameters of different real water samples.

Sample	pH	COD (mg L^{-1})	TN (mg L^{-1})	NH_3−N (mg L^{-1})	NO_3−N (mg L^{-1})	TP (mg L^{-1})	Chroma
RW	8–9	150–250	10–20	5–15	0.5–2	3–5	50–200
WWTP effluent	6–9	1–20	3–6	0.5–1	3–6	0.5–1	10–50
PDIP effluent	7–9	50–100	4–7	0.5–2	2–6	0.5–2	150–250

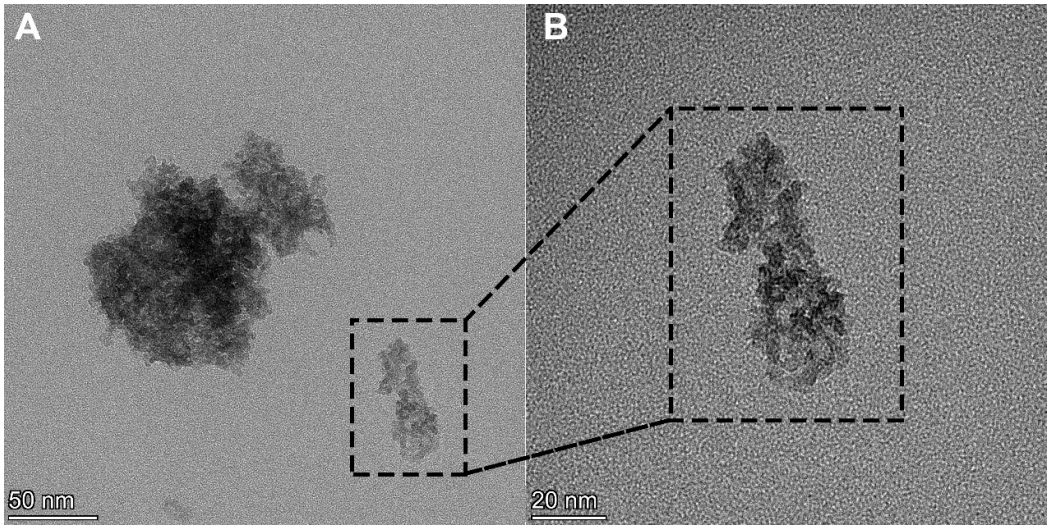

Figure S1. TEM images of Fe/Mn@γ−Al2O3 (**A**) and a partial enlargement (**B**).

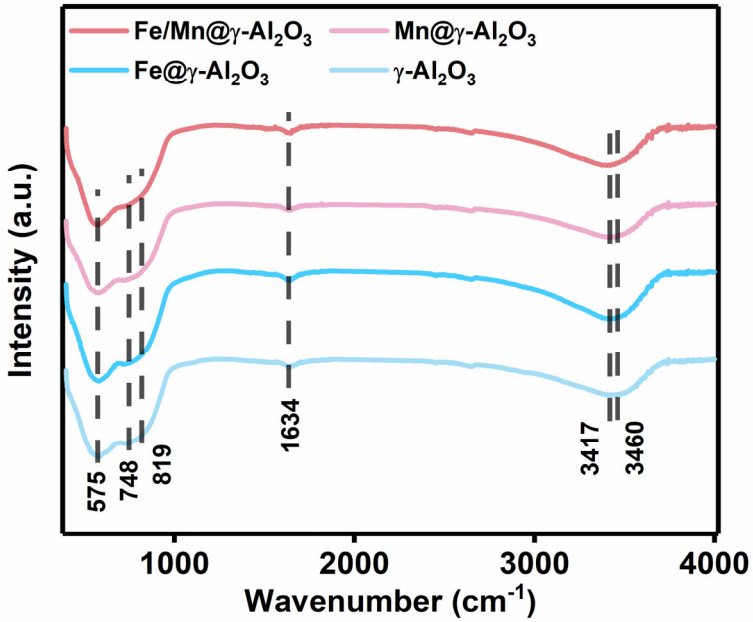

Figure S2. FT−IR spectra of γ−Al_2O_3, Fe@γ−Al_2O_3, Mn@γ−Al_2O_3, and Fe/Mn@γ−Al_2O_3.

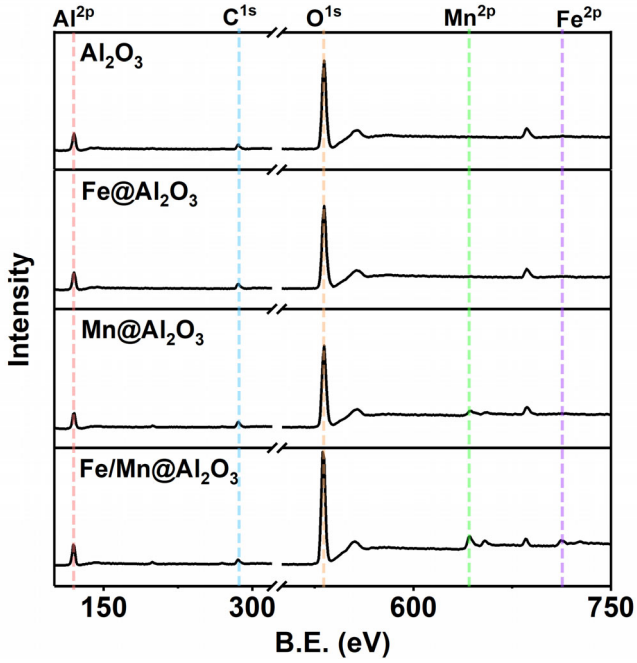

Figure S3. The survey spectrum of XPS spectra of $NiCo_2O_4$ before catalytic ozonation.

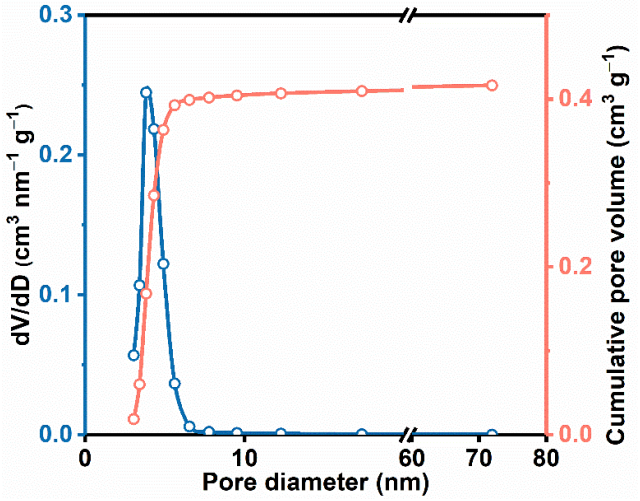

Figure S4. The corresponding pore size distribution in nitrogen adsorption and desorption isotherms.

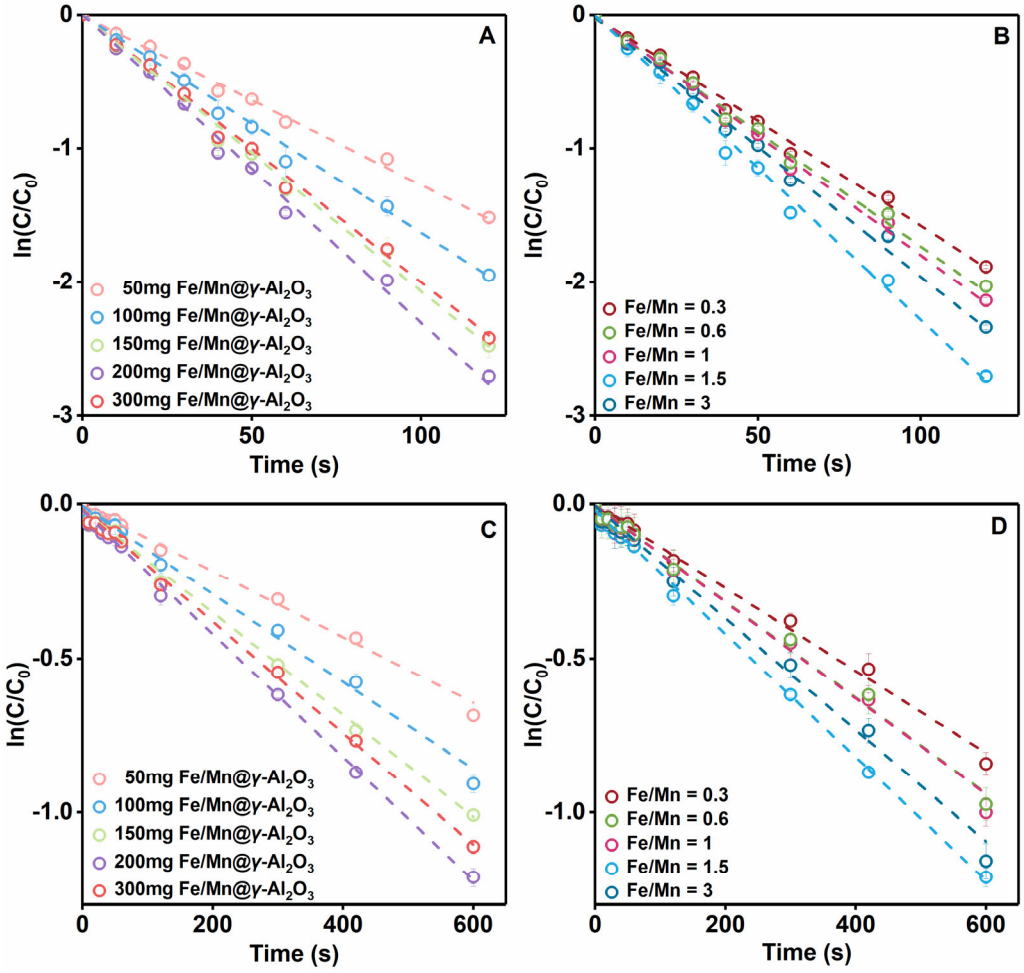

Figure S5. Influence of (**A**), (**C**) Fe/Mn@γ−Al_2O_3 dose and (**B**), (**D**) the ratio of iron to manganese in the catalyst on DMP and 1−NP decomposition. Conditions: [O_3] = 0.04 mM, [catalyst] = 50−300 mg L^{-1}, the molar ratio of Fe/Mn = 0.3−1.5, [DMP]/[1−NP] = 50 μM, 2 mM phosphate buffer.

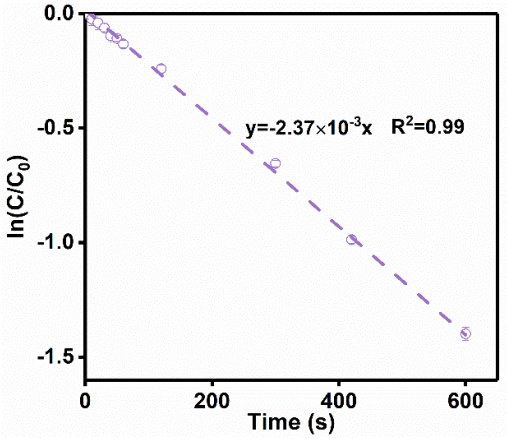

Figure S6. The degradation of 1−NP under ozonation in presence of FFA. Conditions: [O_3] = 0.02 mM, [FFA] = 100 mM, [1−NP] = 50 μM, pH = 7.0 ± 0.1 with 2 mM phosphate buffer.

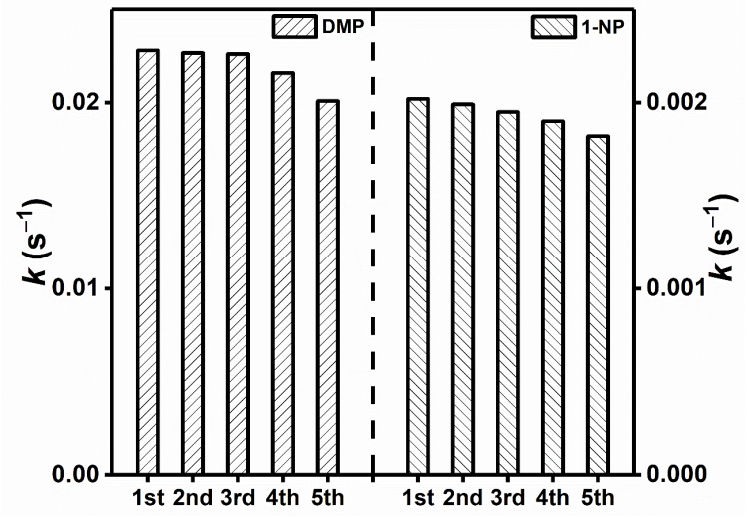

Figure S7. DMP and 1−NP removal rate constants during the reuse of Fe/Mn@γ−Al_2O_3 in catalytic ozonation system.

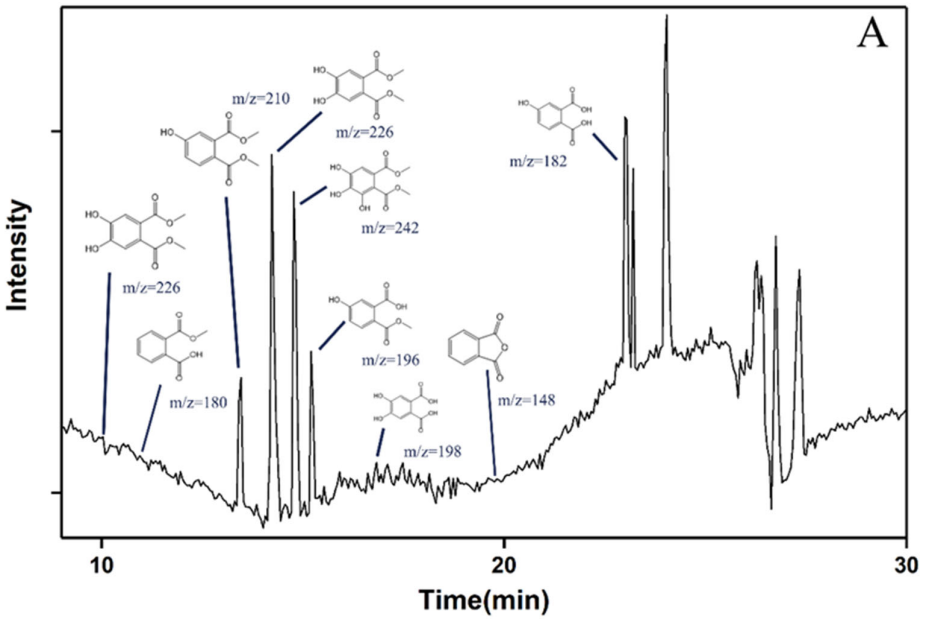

Figure S8. LC−MS total ion chromatograms for DMP degradation products.

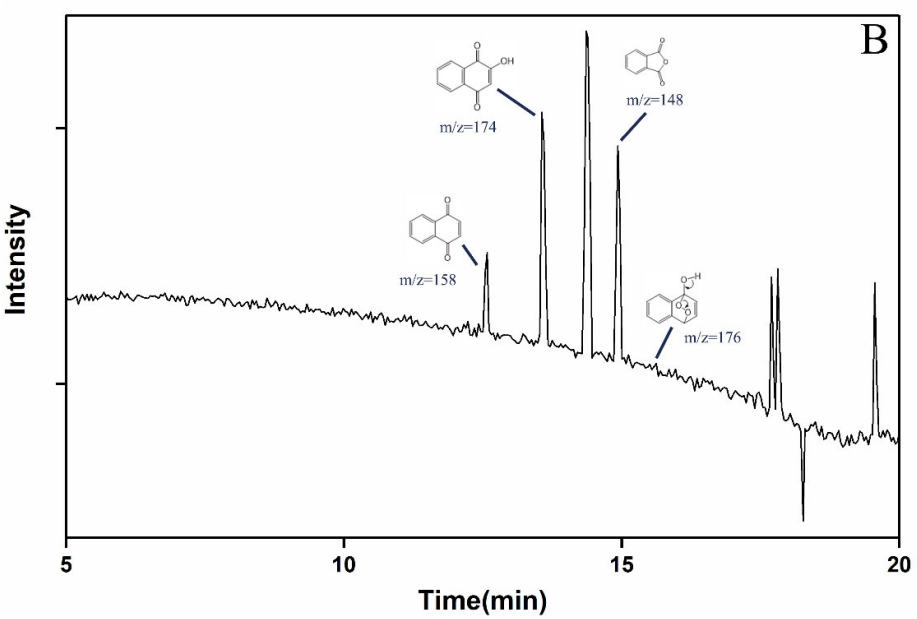

Figure S9. LC–MS total ion chromatograms for 1–NP degradation products.

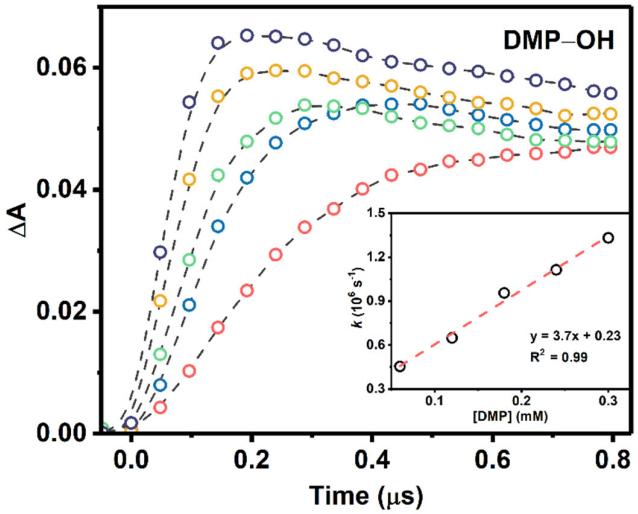

Figure S10. Growth kinetics of DMP–OH adducts at 320 nm with different concentrations of DMP (0.02–0.3 mM) determined by using a laser flash photolysis system. The inset is the plot of the first–order formation rate constants of DMP–OH adducts vs. DMP concentrations.

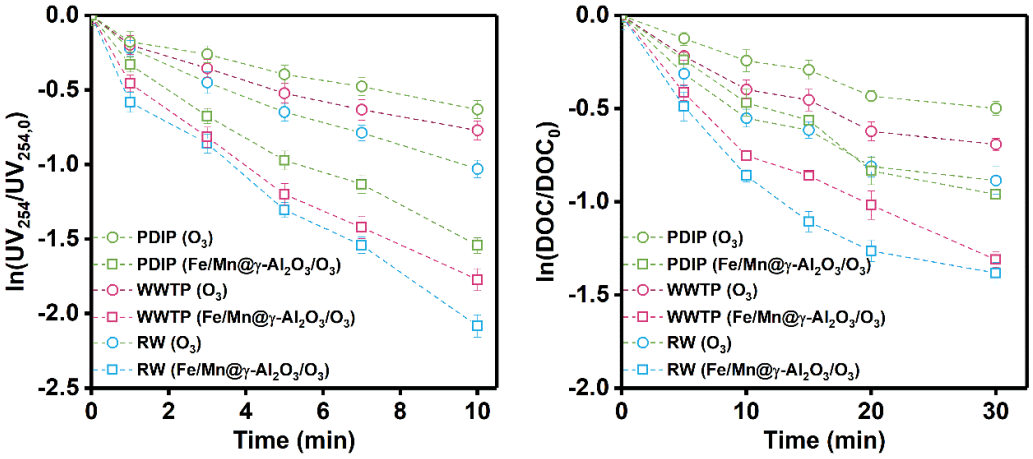

Figure S11. The removal of UV_{254} and DOC during the catalytic ozonation in the real water samples. Conditions: [O_3] = 0.02 mM, [catalyst] = 200 mg L^{-1}, the molar ratio of Fe/Mn = 1.5.

Reference

1. H.Bader; J.Hoigné. Determination of ozone in water by the indigo method. Water Res. **1981**, *15*, 449–456.
2. Rakness, K.L.; Wert, E.C.; Elovitz, M.; Mahoney, S. Operator−Friendly Technique and Quality Control Considerations for Indigo Colorimetric Measurement of Ozone Residual. Ozone−Sci Eng **2010**, *32*, 33–42.
3. Hoigne, J.; Bader, H. Rate constants of reactions of ozone with organic and inorganic compounds in water. I. Non−dissociating organic compounds. Water Res. **1983**, *17*, 173–183.
4. Nonell, S.; Sese, M.L.; Martire, D.O.; Braslavsky, S.E.; Trull, F.R. Polymer bound pyrrole compounds. VI. Photophysical properties of monomeric models for polystyrene−bound porphyrins. Photochem. Photobiol. **1991**, *53*, 185–193.
5. Haag, W.R.; Hoigne', J.; Gassman, E.; Braun, A. Singlet oxygen in surface waters—Part I: Furfuryl alcohol as a trapping agent. *Chemosphere* **1984**, *13*, 631–640, https://doi.org/10.1016/0045−6535(84)90199−1.
6. Gottfried, V.; Kimel, S. Temperature effects on photosensitized processes. *J. Photochem. and Photobiol. B: Biol.* **1991**, *8*, 419–430, https://doi.org/10.1016/1011−1344(91)80116−y.
7. Savel'eva, O.S.; Shevchuk, L.G.; Vysotskaya, N.A. Reactivity of substituted benzenes, furans, and pyridines to hydroxyl radicals. J. Org. Chem. **1973**, *9*, 759–761.
8. Lei, Y.; Lu, J.; Zhu, M.; Xie, J.; Peng, S.; Zhu, C. Radical chemistry of diethyl phthalate oxidation via UV/peroxymonosulfate process: Roles of primary and secondary radicals. *Chem. Eng. J.* **2019**, *379*, 122339, https://doi.org/10.1016/j.cej.2019.122339.
9. Wen, G.; Ma, J.; Liu, Z.Q.; Zhao, L. Ozonation kinetics for the degradation of phthalate esters in water and the reduction of toxicity in the process of O3/H2O2. J Hazard Mater. **2011**, *195*, 371–377.
10. Mvula, E.; von Sonntag, C. Ozonolysis of phenols in aqueous solution. Org. and Biomol. Chem. **2003**, *1*, 1749–1756.
11. Adams, G.E.; Michael, B.D. Pulse radiolysis of benzoquinone and hydroquinone. Semiquinone formation by water elimination from trihydroxy− cyclohexadienyl radicals. Trans. of Faraday Soc. **1967**, *63*, 1171–1180.
12. Greenstock, C.; Ruddock, G. Determination of superoxide (O2−) radical anion reaction rates using pulse radiolysis. *Int. J. Radiat. Phys. Chem.* **1976**, *8*, 367–369, https://doi.org/10.1016/0020−7055(76)90082−6.
13. Buxton, G.V.; Greenstock, C.L.; Helman, W.P.; Ross, A.B. Critical review of rate constants for reactions of hydrated electrons, hydrogen atoms and hydroxyl radicals (·OH/·O−) in aqueous solution. J. Phys. and Chem. Ref. Data **1988**, *17*, 513–886.